

Motion-inductive Self-supervised Object Discovery in Videos

Shuangrui Ding¹ Weidi Xie¹ Yabo Chen¹

Rui Qian² Xiaopeng Zhang³ Hongkai Xiong¹ Qi Tian³

¹Shanghai Jiao Tong University ²The Chinese University of Hong Kong ³Huawei Inc.

{dsr1212, weidi, chenyaobo, xionghongkai}@sjtu.edu.cn

qr021@ie.cuhk.edu.hk zxp@history@gmail.com tian.qi1@huawei.com

Abstract

In this paper, we consider the task of unsupervised object discovery in videos. Previous works have shown promising results via processing optical flows to segment objects. However, taking flow as input brings about two drawbacks. First, flow cannot capture sufficient cues when objects remain static or partially occluded. Second, it is challenging to establish temporal coherency from flow-only input, due to the missing texture information. To tackle these limitations, we propose a model for directly processing consecutive RGB frames, and infer the optical flow between any pair of frames using a layered representation, with the opacity channels being treated as the segmentation. Additionally, to enforce object permanence, we apply temporal consistency loss on the inferred masks from randomly-paired frames, which refer to the motions at different paces, and encourage the model to segment the objects even if they may not move at the current time point. Experimentally, we demonstrate superior performance over previous state-of-the-art methods on three public video segmentation datasets (DAVIS2016, SegTrackv2, and FBMS-59), while being computationally efficient by avoiding the overhead of computing optical flow as input.

1. Introduction

Representing the visual scene with objects as the basic elements has long been considered a fundamental cognitive ability of the intelligent agent, for it enables understanding and interaction with the world more efficiently, for example, combinatorial generalization in novel settings [58]. Although it remains somewhat obscure at the level of neurophysiology on exactly how humans discover the objects in a visual scene in the first place, it is a consensus that motion seems to play an indispensable role in defining and discovering the objects from the scene. For example, in 1923, Wertheimer introduced the common fate principle that elements moving together tends to be perceived as a

group [66]; while later Gibson claimed the independent motion has even been treated as one attribute to define an object visually [21]. Grounded on the above assumptions, the recent literature has witnessed numerous works with different models proposed for segmenting the moving objects via unsupervised learning [42, 70–72].

Exploiting optical flows for object discovery naturally incurs two critical limitations: *First*, objects in videos may stop moving or be partially occluded at any time point, leaving no effective cues for their existence in the flow field; *Second*, computing optical flow from a pair of frames refers to a lossy encoding procedure, that poses a significant challenge for establishing temporal coherence, due to the lack of effective texture information. In contrast, adopting RGB frame sequences poses a few clear advantages. The most obvious one is that, while objects do not necessarily move all the time, the property of temporal coherence in RGB space naturally guarantees a preliminary understanding of object permanence; Additionally, the rich textures in the appearance stream give more distinctive patterns than those in motion, allowing to better identify and distinguish the different objects. Last but not least, processing RGB streams still enables a faster processing speed than using optical flow.

In this paper, our goal is to train a video segmentation model that can discover the moving objects within a sequence of RGB frames, in the form of segmentation. In specific, our proposed model first encodes consecutive frames independently, into a set of frame-wise visual features, that is followed by a temporal fusion with a Transformer encoder. To localise the moving objects, we randomly pair the visual features from two frames and pass them into a frame comparator module, effectively establishing the relative motion between frames. Inspired by [70], we decode the motion features into optical flows with a dual-layered representation, with the opacity weight of each layer treated as the segmentation mask. At training time, we exploit an off-the-shelf optical flow estimator, *e.g.*, RAFT [57], as the induction for flow reconstruction. To develop the property

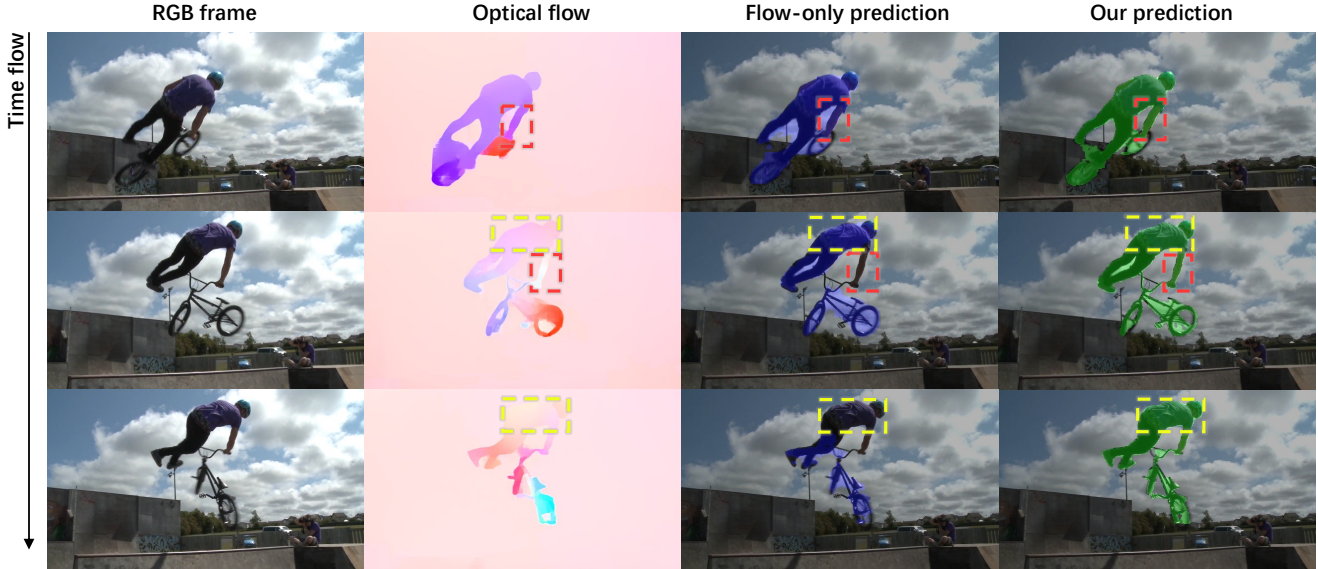


Figure 1. Illustration about Bicycle Motocross (BMX) sequence on SegTrackv2 [38]. The red boxes and the yellow boxes refer to the arm and the back of the player, respectively. Flow-only method [70] fails to track the same region in a temporal consistent fashion since it derives the foreground region directly from current optical flow. However, our methodology of processing a RGB video clip develops a sense of object permanence and solves the issue.

of object permanence, we enforce a temporal consistency on the inferred segmentation masks, which encourages the model to mine effective texture information from the RGB sequence and keep track of the objects even if they may be static at the current time point.

In short, we summarize the contributions in this paper: *First*, we introduce the **Motion-inductive Object Discovery (MOD)** model, a simple architecture for discovering the moving objects in videos, by directly processing a set of consecutive RGB frames. *Second*, we propose a self-supervised proxy task that is used to train the architecture without relying upon any manual annotation. To overcome the challenge from flow-based methods, *i.e.*, objects may stay static or move slowly, we adopt a random-paired policy and restrain the temporal consistency. *Third*, we conduct a series of ablation studies to validate each key component of our method, such as the temporal consistency of random-paired flow. While evaluating three public benchmarks, we demonstrate superior performance over existing approaches on DAVIS2016 [54], SegTrackv2 [38], and FBMS-59 [51], with considerable speed-up during the inference procedure.

2. Motion-inductive Object Discovery Model

In this section, we detail our Motion-inductive Object Discovery (MOD) model, which processes a set of consecutive RGB frames and automatically discovers the moving objects in the form of segmentation. An overview of the training procedure can be seen in Figure 2, where the

visual features computed from individual frames are temporally fused, and randomly paired together, for decoding the optical flows between two corresponding frames. Taking inspiration from the motion grouping [70], we also adopt a dual-layered representation for the output flow, with the foreground and background flows being reconstructed separately, and later composited with the inferred opacity masks (soft segmentation). In the following section, we will detail each key component in our proposed architecture.

2.1. Spatial-temporal Visual Encoder

To start with, our model takes a short video clip as input, *i.e.*, $v = \{x_1, \dots, x_T\}$, $v \in \mathbb{R}^{T \times H \times W \times 3}$, consisting of a set of RGB frames, the frame-wise visual representations are computed with a shared visual encoder Φ_{enc} . Formally, the output feature map o_t at timestamp t ($1 \leq t \leq T$) can be obtained:

$$o_t = \Phi_{\text{enc}}(x_t) \in \mathbb{R}^{h \times w \times d}, \quad (1)$$

where h, w, d denotes the dimension of the height, width, and channel, respectively. Till this point, to build the temporal dependency between multiple visual frames, a global fusion module is introduced, via a standard Transformer Encoder layer:

$$\{\tilde{o}_1, \dots, \tilde{o}_T\} = \Phi_{\text{temp}}(\{o_1 + \text{pe}_1, \dots, o_T + \text{pe}_T\}), \quad (2)$$

where pe refers to the learnable spatial-temporal positional encodings, and the output $\tilde{o}_t \in \mathbb{R}^{h \times w \times d}$ remains the same dimension as input.

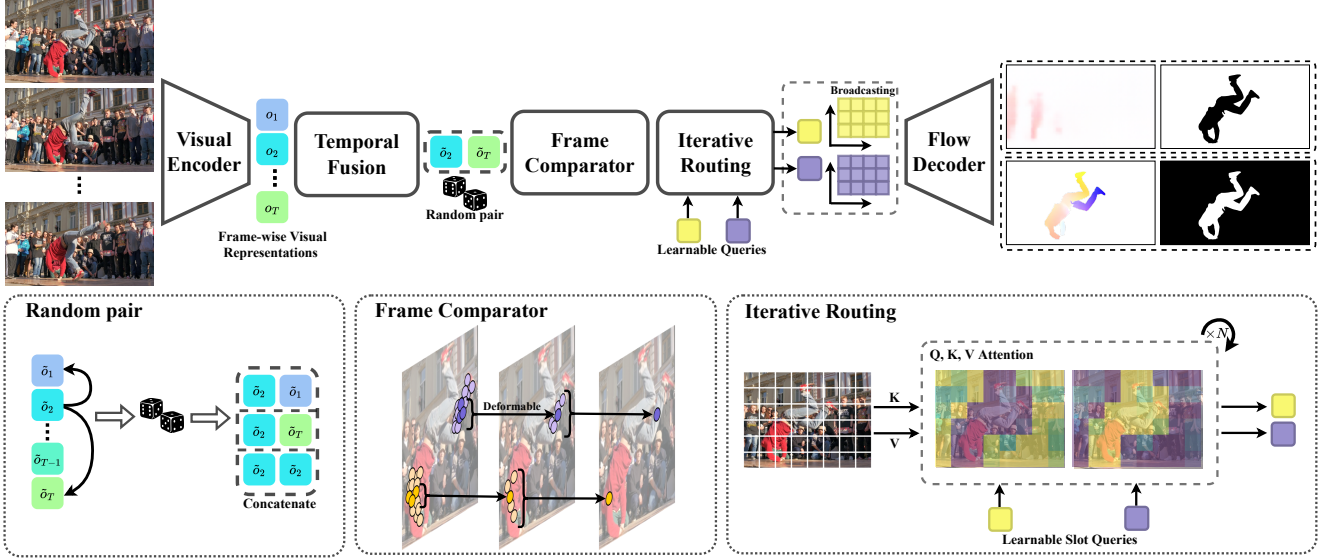


Figure 2. **Model architecture.** Our model first extracts spatial features of consecutive frames by the visual encoder. To jointly model the temporal relation, we aggregate and interact among the multi-frame features with late-fusion. We randomly pair two frames’ visual representations and pass them into the frame comparator to encode relative motion. Then, we decode the flow from random-paired frames. Through iterative routing, we adopt a dual-layer representation for the flow reconstruction, *i.e.*, outputting the foreground and background flows separately, and composing them with inferred opacity weights. The whole training procedure does not require supervision from any mask annotations.

By taking the multiple RGB frames as input, our proposed visual encoder can explicitly consider the temporal coherence within the video clip. **Note that**, such seemingly simple design poses two critical differences from previous work on motion-driven object discovery [70, 72], where only frame-wise optical flow is adopted: *First*, using RGB frames as input can drastically reduce the computation latency at inference time. The throughput of our model without computing dense optical flow reaches round **100 fps** on a standard 32GB Tesla V100 GPU while prior works need to calculate flow at first. RGB provides more semantic information than flows for the model to exploit, *i.e.*, including not only the object’s shape but also its texture. *Second*, processing multiple frames contributes to the development of a sense of object permanence within the video clip, *i.e.*, the understanding that items or people still exist even when they cannot be perceived explicitly. Therefore, even though the objects in videos may stop moving or be partially occluded at any time point, they can still be effectively segmented with the temporal cues.

2.2. Random-paired Frame Comparator

Till this point, we consider building the relative motion between any two visual frames within the video clip, from reference frame i to target frame j , *i.e.*, $f_{i \rightarrow j}$. In specific, we select the visual representation of the two corresponding frames, *i.e.*, \tilde{o}_i and \tilde{o}_j , concatenate them along the feature

dimension, and feed it into a comparator module:

$$f_{i \rightarrow j} = \Phi_{\text{comp}}(\text{concat}(\tilde{o}_i, \tilde{o}_j)) \in \mathbb{R}^{h \times w \times d}, \quad (3)$$

where $\Phi_{\text{comp}} : \mathbb{R}^{2d} \rightarrow \mathbb{R}^d$ consists of multiple deformable convolutional layers [76] followed by a series of Transformer Encoders, that dynamically construct the feature representation for later estimating relative motion between frames while reducing the feature dimensions at the same time.

Discussion. With such a design of random-paired frame comparator, our MOD is capable of modeling the relative motion between any two randomly sampled frames out of the video clip (T frames), accounting for a total of T^2 frame pairs for forward, backward, single, or multi-step motions. Note that, we do not distinguish the case of $i \neq j$ and $i = j$. Specifically, the former encourages the model to discover the relative motion between two different frames, while the latter refers to an extreme case that neither objects nor camera is moving, and no motion cues are available, thus enforcing the model to discover objects via temporal coherence, *i.e.*, objects that moves in any frame along the video should also be discovered in static frames.

2.3. Dual-layered Flow Decoder

To decode the features into the form of optical flow, we adopt several slot attention layers [43] with two learn-

able queries, *i.e.*, termed as slot vectors, iteratively attending the output visual features from the comparator, and decoded into the optical flow between any two frames with a dual-layered representation. In detail, a slot attention module acts similarly to a Transformer Decoder, with the only exception being that the normalisation is computed along the slot side, thus each slot competes to take over the pixels. In each iteration, given two slot vectors as $S \in \mathbb{R}^{2 \times d}$ and visual feature maps $\tilde{o}_t \in \mathbb{R}^{hw \times d}$, we use three linear projections to compute the query, key and value, *i.e.*, $Q \in \mathbb{R}^{2 \times d}$, $K, V \in \mathbb{R}^{hw \times d}$. Thereafter, we can obtain the weights matrix $W \in \mathbb{R}^{2 \times hw}$ and normalise along the slot dimension, *i.e.*,

$$\begin{aligned} \widetilde{W}_{s,\cdot} &= \exp(W_{s,\cdot}) / \sum_l \exp(W_{l,\cdot}), \\ \text{where } W &= \frac{1}{\sqrt{d}} QK^T. \end{aligned} \quad (4)$$

Then, we gain the next iteration’s slot vectors by aggregating the values V and passing them into a Gated Recurrent Unit (GRU) [10], *i.e.*,

$$\begin{aligned} S &:= \text{GRU}(\text{inputs} = AV, \text{states} = S), \\ \text{where } A_{\cdot,s} &= \frac{\widetilde{W}_{\cdot,s}}{\sum_l \widetilde{W}_{\cdot,l}} \in \mathbb{R}^{2 \times (h \times w)}. \end{aligned} \quad (5)$$

We iterate the whole routing process for N times. In this way, the entities of similar RGB and flow patterns are grouped together and distinct pixels are separated by two slots. Eventually, we broadcast the final outputted slots into $G = \{G^s \in \mathbb{R}^{h \times w \times d}\}_{s=1}^2$ added with learnable spatial positional embeddings to construct the optical flow. A flow decoder Φ_{dec} consisting Transformer encoders and up-sampling layers takes the slot grids as input, and outputs dual layers of optical flows $\{\tilde{I}^s \in \mathbb{R}^{H \times W \times 3}\}_{s=1}^2$ ¹ and their opacity weights $\{\alpha^s \in \mathbb{R}^{H \times W \times 1}\}_{s=1}^2$:

$$\{\tilde{I}^s, \alpha^s\}_{s=1}^2 = \Phi_{\text{dec}}(G), \quad (6)$$

where $\alpha^s \in [0, 1]^{H \times W \times 1}$ is normalized across two slots via softmax function. For a given frame pair (i, j) , their relative flow $\tilde{I}_{i \rightarrow j}$ can be computed via:

$$\tilde{I}_{i \rightarrow j} = \sum_{s=1}^2 \alpha_{i \rightarrow j}^s \otimes \tilde{I}_{i \rightarrow j}^s, \quad (7)$$

where \otimes denotes the element-wise multiplication. At inference time, we adopt the binarized opacity weights α^s as the object segmentation masks.

¹Note that following the common practise, we also output 3-channel RGB images, that refers to a transformation from the traditional 2-channel optical flow based on the color wheel proposed in [56].

2.4. Training

In this section, we describe the training procedure for the proposed model, on the raw videos without using manual annotations for the object segmentations. In general, the training loss is composed of three components, namely, flow reconstruction, temporal consistency, and entropy minimisation.

Flow Reconstruction. As the main objective for optimisation, we use the flow reconstruction, where we adopt an off-the-shelf optical flow estimator, for example, RAFT [57], to estimate the flow between any two frames in the video. We minimise the discrepancy between the dual-layer flow reconstruction and the output from the existing flow estimator:

$$\mathcal{L}_{\text{recon}}^{i \rightarrow j} = \frac{1}{|\Omega|} \sum_{u \in \Omega} |I_{i \rightarrow j}(u) - \tilde{I}_{i \rightarrow j}(u)|_2, \quad (8)$$

where $\Omega = \{1, \dots, H\} \times \{1, \dots, W\}$ represents the spatial lattice, and a $|\cdot|_2$ denotes the L2 norm. In practice, the reconstruction constraint for zero flow when $i = j$ is dropped due to the distribution gap between dynamic flow and static flow, resulting in the divergence of the training. **Note that**, flow estimator is only used for model training, at inference time, our proposed architecture directly processes the RGB video clips.

Temporal Consistency. In order to build up temporal consistency within the input video, the pair of motion embeddings $f_{i \rightarrow j}, f_{i \rightarrow k}$ that starts from the same reference frame i , are passed through the flow decoder to reconstruct the optical flow between two corresponding frames. Note that, as $1 \leq j, k \leq T$ are randomly sampled at every training iteration, the output flow will refer to the motion at a different pace. However, the predicted alpha weights for flow composition denote the soft segmentation for the same objects in the i -th frame, thus remaining consistent. In specific, the two inferred masks $\{\alpha_{i \rightarrow j}^s\}_{s=1}^2, \{\alpha_{i \rightarrow k}^s\}_{s=1}^2$ are enforced to pull closer by minimising mean-squared error $\mathcal{L}_{\text{cons}}$, *i.e.*,

$$\mathcal{L}_{\text{cons}} = \frac{1}{T} \sum_{i=1}^T \mathcal{L}_{\text{cons}}^i, \quad (9)$$

$$\text{where } \mathcal{L}_{\text{cons}}^i = \frac{1}{2|\Omega|} \sum_{u \in \Omega} \sum_{s=1}^2 |\alpha_{i \rightarrow j}^s(u) - \alpha_{i \rightarrow k}^s(u)|^2.$$

Entropy Minimisation. Lastly, we impose a pixel-wise entropy regularisation on inferred masks, that is zero if the alpha channels are one-hot, and maximum when they are of equal probability. Intuitively, this helps encourage the

masks to be binary, which aligns with our goal in obtaining segmentation masks:

$$\mathcal{L}_{\text{entro}}^{i \rightarrow j} = \frac{1}{2|\Omega|} \sum_{u \in \Omega} \sum_{s=1}^2 -\alpha_{i \rightarrow j}^s(u) \log(\alpha_{i \rightarrow j}^s(u)). \quad (10)$$

Total Loss. Accordingly, we rewrite aforementioned reconstruction loss $\mathcal{L}_{\text{recon}}$ and entropy regularization $\mathcal{L}_{\text{entro}}$ in summed version:

$$\mathcal{L}_{\text{recon}} = \frac{1}{2T} \sum_{i=1}^T \mathcal{L}_{\text{recon}}^{i \rightarrow j_i} + \mathcal{L}_{\text{recon}}^{i \rightarrow k_i}, \quad (11)$$

$$\mathcal{L}_{\text{entro}} = \frac{1}{2T} \sum_{i=1}^T \mathcal{L}_{\text{entro}}^{i \rightarrow j_i} + \mathcal{L}_{\text{entro}}^{i \rightarrow k_i}. \quad (12)$$

The total loss for training our model can thus be computed as:

$$\mathcal{L}_{\text{tot}} = \lambda_r \mathcal{L}_{\text{recon}} + \lambda_e \mathcal{L}_{\text{entro}} + \lambda_c \mathcal{L}_{\text{cons}}, \quad (13)$$

where we set $\lambda_r = 100$, $\lambda_e = \lambda_c = 0.01$ at the beginning of the training. We notice the model to be fairly robust to these hyper-parameters.

3. Experimental Setup

In the experiments setup, we first introduce the benchmarks and then elaborate on implementation details.

3.1. Datasets

We benchmark on three popular datasets designed for video object segmentation. **DAVIS2016** [54] consists of 50 high quality videos, 3455 frames in total. Every frame is annotated with a pixel-accurate segmentation mask. **SegTrackv2** [38] contains 14 sequences and 947 fully-annotated frames. Each sequence involves 1-6 moving objects and presents challenges including motion blur, appearance change, complex deformation, occlusion, slow motion, and interacting objects. **FBMS-59** [51] has 59 sequences with greatly varied resolution and annotates every 20th frame. Many sequences contain multiple moving objects. Following previous evaluation metric [68, 72], we merge objects of SegTrackv2 and FBMS-59 into one single object for video object segmentation. We evaluate the pixel-wise segmentation through Jaccard index \mathcal{J} , also called Intersection over Union (IoU). Following prior arts [70, 72], we compute the mean per frame over the test set and merge multi-object annotation into single unified segmentation.

3.2. Implementation Details

For data input, we sample $T = 7$ consecutive frames as the input clip. Each frame is resized to 192×384 and the estimated optical flow is computed by RAFT [57], which is pre-trained on the synthetic dataset [48].

To compute spatial-temporal visual representation, we adopt the first three stages of a SwinV2-T as the frame encoder Φ_{enc} , which is then followed by a standard Transformer Encoders with 8 heads [61] as temporal fusion module Φ_{temp} . For the frame comparator Φ_{comp} , we use two deformable convolutional layers in the company with three standard Transformer Encoders with 8 heads to process the pixel transformation. Then, we choose $N = 5$ iteration in total for the iterative routing in slot attention. Lastly, we utilize three stages of SwinV2 blocks with the linear patch expanding layers as the flow decoder Φ_{dec} [8].

As for training, we adopt AdamW optimizer [44] with learning rate 4×10^{-5} . The model is trained from scratch without any pretrained weights, for a total of 300k iterations. At inference time, we adopt the temporal sliding window to ensemble the segmentation masks. We average the resultant masks obtained by the whole temporal segments. We propose two protocols to evaluate our results. Besides measuring the masks without any post-processing, we also apply **test-time adaptation** with the help of the self-supervised DINO-pretrained ViT [9]. Without any fine-tuning, the pretrained ViT can propagate the masks as noisy annotations to the whole frames in the same manner as CRW [25]. We refine the masks further with CRF [33]. For more detailed technical information, please refer to the supplementary materials.

4. Results

In this section, we compare primarily with several top-performing approaches trained without human annotations, for example, OCLR [68], MG [70], SIMO [36], CIS [72], etc. However, as the architecture, modality, input resolution, and post-processing protocols are all different, we try our best to conduct the comparison as fairly as possible.

4.1. Ablation Study

We conduct all ablation studies on DAVIS2016 and vary one variable each time, as shown in Table 1.

Temporal Fusion Φ_{temp} and Frame Comparator Φ_{comp} . As shown by Ours-A and Our-C, the performance degrades significantly without temporal fusion, demonstrating the importance of building up global temporal dependency. Also, indicated by Ours-B, we find the model fails to converge when removing the component of frame comparator Φ_{comp} . It meets expectations because frame comparator Φ_{comp} is the sole module in charge of relative motion estimation. Without it, the model cannot reconstruct optical flow thus leading to divergence.

Number of Frames T . While comparing Ours-A, Ours-D, and Ours-E, there is a clear trend that increasing the

Model	Φ_{temp}	Φ_{comp}	T	$\mathcal{L}_{\text{cons}}$	$\mathcal{L}_{\text{entro}}$	DAVIS($\mathcal{J} \uparrow$)
Ours-A	✓	✓	7	✓	✓	73.9
Ours-B	-	✗	7	✓	✓	fail
Ours-C	✗	✓	7	✓	✓	68.3
Ours-D	✓	✓	3	✓	✓	66.4
Ours-E	✓	✓	5	✓	✓	68.2
Ours-F	✓	✓	7	✗	✗	60.4
Ours-G	✓	✓	7	✗	✓	65.6
Ours-H	✓	✓	7	✓	✗	69.5

Table 1. Ablation studies on temporal fusion (Φ_{temp}), frame comparator (Φ_{comp}), the number of input frames (T), temporal consistency ($\mathcal{L}_{\text{cons}}$), and entropy loss ($\mathcal{L}_{\text{entro}}$).

frame number boosts the segmentation quality, which coincides with our intuition that incorporating a wider temporal receptive field can enhance the sense of temporal coherence and object permanence. Due to the limited computational memory, we only set $T = 7$ as the maximum frame number in the paper. A promising performance is expected when inputting more frames.

Temporal Consistency $\mathcal{L}_{\text{cons}}$ and Entropy Regularisation $\mathcal{L}_{\text{entro}}$. Lastly, comparing Ours-G and Ours-A, we observe that the performance increases considerably with temporal consistency. It manifests the validity of our design motivation, temporal consistency conduces to persistently tracking the object. The entropy regularisation is also indispensable shown by Ours-H and Ours-A.

4.2. Comparison with State-of-the-art

We show the comparison with state-of-the-art in Table 2. On DAVIS2016, MOD achieves 73.9% mIOU without any post-processing, exceeding MG [70] by a large margin (+5.8%). Compared to the latest method OCLR [68] which fabricates a synthesized dataset to train its model, our method still surpasses it only using the information of the DAVIS dataset itself. On another two benchmarks SegTrackv2 and FBMS-59, MOD also beats MG [70], which only leverages single-step flows to decompose foreground and background, by +3.6% and +8.2%, respectively. The superior experimental results demonstrate that our methodology of multi-frame reasoning benefits moving object discovery. Furthermore, equipped with DINO-pretrained ViT, a further performance gain is observed on all three benchmarks, which is even more competitive with current supervised approaches.

4.3. Qualitative Results

In Figure 3, we present several qualitative illustrations of the model. It can be seen that our results are robust to the

noticeable background flow signal (drift-chicane sequence in the second column) and estimate more accurate boundaries when single-step foreground flow cannot represent exact object shape (breakdance and dance-twirl sequences in middle) compared to MG [70]. It demonstrates inferring the masks by associating a bunch of RGB features well resolves the limitation of the usage of flow. Moreover, in virtue of temporally consistent cues, our model handles occlusion well shown in the libby sequence at the rightmost column, which could be hard for the flow-only method to maintain the object shape constantly.

4.4. Limitations

Though we demonstrate that associating multiple frames stimulates the comprehensive sense of objectness, which is proved by the superior experimental performance across the prior arts, there still exist limitations and room for improvement. *First*, our method uses a number of consecutive frames, which challenges computational memory. How to utilize pretrained features for reducing training expenses would be meaningful. *Second*, how to segment multiple objects remains unexplored. It will be promising to exploit the semantic information from RGB to discriminate different foreground objects. We leave them as the feature work. Despite these limitations, the approach has convincingly manifested the value of considering textural information and processing RGB frames as a whole.

5. Related Work

Video Object Segmentation. How to segment objects coherently in one video sequence has extended the topic of instance segmentation in the image. There is a great amount of work about video object segmentation (VOS) in recent decades [1, 7, 7, 14, 19, 23, 24, 28, 35, 40, 47, 52, 53, 62, 62]. Recently, the research on getting rid of the dense annotation and designing more effective self-supervised algorithms has attracted more and more interest in the computer vision community including VOS [25, 31, 34, 39, 46, 63, 64, 69]. For VOS, there are two mainstream protocols to evaluate the learned model. One is semi-supervised video object segmentation, the other is unsupervised video object segmentation. Given the first-frame mask of the objects of interest, semi-supervised VOS tracks those objects in subsequent frames, while unsupervised VOS directly segments the most salient objects from the background without any reference. These two protocols are defined in the inference phase, meaning methods could leverage ground truth annotations in the training stage. In this paper, we don’t use any kinds of manual annotations for either training or evaluation.

Motion Segmentation. As the name suggests, the aim of motion segmentation is to discover moving objects. One

Model	Training		Inference		\mathcal{J} (Mean) \uparrow		
	HA	Sup.	RGB	Flow	DAVIS2016	SegTrackv2	FBMS-59
SAGE [65]	\times	None	\checkmark	\checkmark	42.6	57.6	61.2
NLC [18]	\times	None	\checkmark	\checkmark	55.1	67.2	51.5
CIS [72]	\times	None	\checkmark	\checkmark	71.5	62.5	63.5
AMD [42]	\times	None	\checkmark	\times	57.8	57.0	47.5
SIMO [36]	\times	None	\times	\checkmark	67.8	62.0	-
MG [70]	\times	None	\times	\checkmark	68.3	58.6	53.1
OCLR [68]	\times	Syn.	\times	\checkmark	72.1	67.6	65.4
MOD (w/o post-processing)	\times	None	\checkmark	\times	73.9	62.2	61.3
MOD (test-time adaptation)	\times	None	\checkmark	\times	79.2	69.4	66.9
FSEG [14]	\checkmark	GT	\checkmark	\checkmark	70.7	61.4	68.4
COSNet [45]	\checkmark	GT	\checkmark	\times	80.5	49.7	75.6
MATNet [75]	\checkmark	GT	\checkmark	\checkmark	82.4	50.4	76.1
D ² Conv3d [55]	\checkmark	GT	\checkmark	\times	85.5	-	-

Table 2. Quantitative comparison on unsupervised video object segmentation. We compare our method on three standard datasets, DAVIS2016, SegTrackv2, and FBMS-59. HA is short for **H**uman **A**nnotation. Sup. refers to the supervision, including None, Synthetic (Syn.), and Ground Truth (GT).

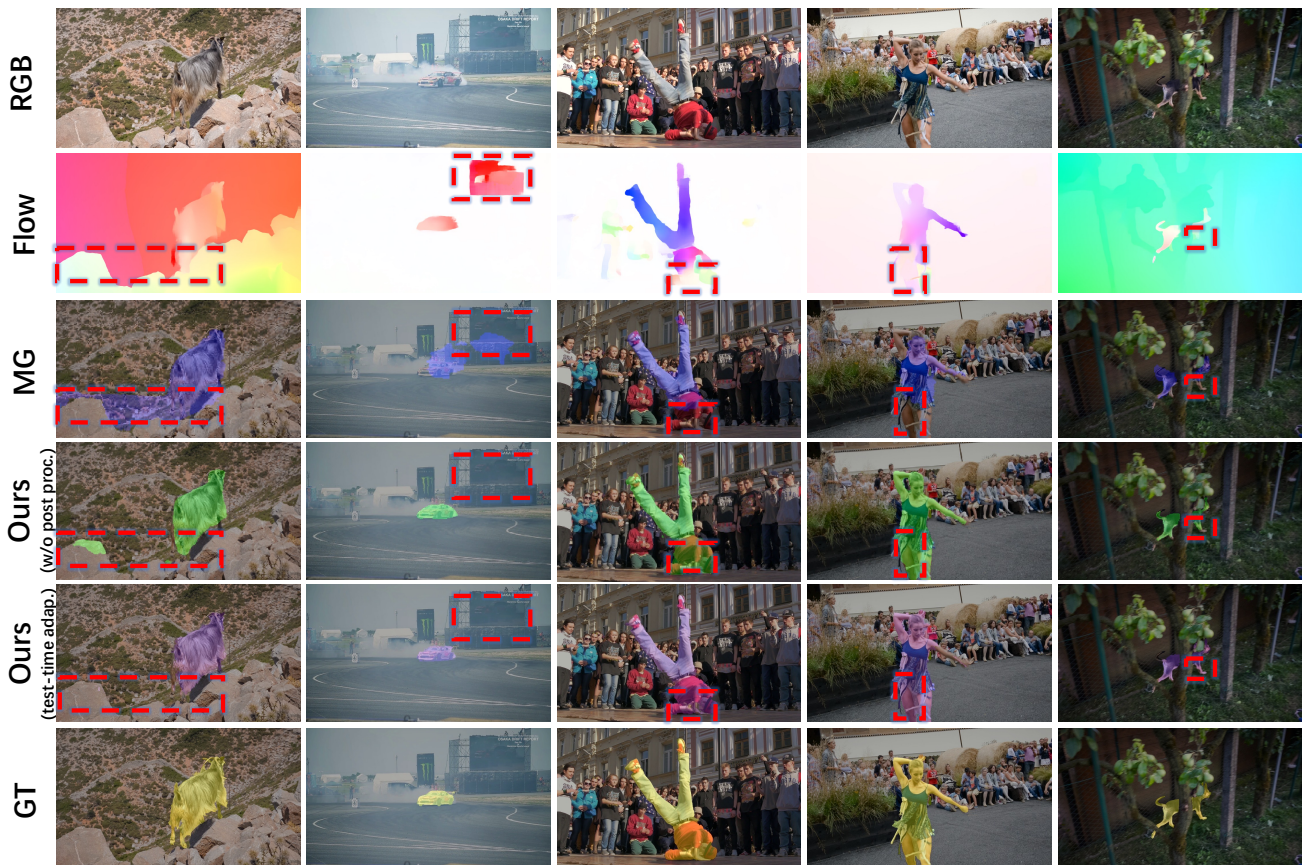


Figure 3. Qualitative results of object video segmentation on DAVIS2016. MG refers to [70]. Red boxes outline the corresponding difference.

line of the work [5, 20, 30, 37, 50, 51] formulates motion as the point trajectory to take advantage of long-range temporal information so that segmentation results can be acquired by grouping the trajectories. Later, deep learning methods take over the area [11, 59, 60, 67, 70, 72]. [60] adopts a two-stream network that ingests both RGB and optical flow. Then they realize a memory mechanism by the convolutional recurrent unit to enhance the visual cues. CIS [72] achieves fully unsupervised motion segmentation which discards the supervision of annotated masks during training. By formulating a min-max game of mutual information, the generator is asked to create foreground segments that are as unrelated as possible to the background. AMD [42] minimizes the warp synthesis error to train appearance and motion pathways without any supervision. MG [70] solely leverages the optical flow to separate the pixels via cross attention mechanism [43]. Recently, OCLR [68] synthesizes a training dataset with multiple moving objects systematically to train their model. Though our method is a bit like MG, the key difference in our work is that we purely take RGB frames as input thus relieving the over-reliance on optical flow and allowing us to segment objects at test time when optical flow is not accessible.

Object Discovery. There is rich literature on identifying salient objects without explicit supervision, known as object discovery. There exist a series of works that aim to learn object-centric representations in images [6, 12, 15–17, 22, 26, 41, 43]. Typically, IODINE [22] develops iterative variational inference to separate different objects. [43] proposes slot attention to iteratively update latent object representations. Further, a line of works [2–4, 13, 27, 29, 31, 32, 49, 70, 73, 74] extend object-centric learning to video domain. Most of these approaches incorporate motion cues into the reconstruction task and perform well in moving object segmentation but perform poorly in processing static objects. While in this work, we adopt slot attention to form optical flow reconstruction bottleneck and perceive both dynamic and static instances through RGB clip input in a temporally consistent way.

6. Conclusion

In this paper, we propose a self-supervised model for video object discovery. The model takes a set of consecutive RGB frames as input and generates the segmentation mask for the moving objects in the video. At training time, the model is tasked to reconstruct the optical flow between any pair of frames, through a layered representation with the opacity channels being treated as the segmentation. To encourage the model to capture the objects even when they may be static at a certain time point, a temporal consistency

loss is enforced on the inferred masks on the randomly-paired frames. As a consequence, we demonstrate superior performance over previous state-of-the-art methods on three public video segmentation datasets (DAVIS2016, SegTrackv2, and FBMS-59), while being computationally efficient by avoiding the overhead of computing optical flow.

References

- [1] Linchao Bao, Baoyuan Wu, and Wei Liu. Cnn in mrf: Video object segmentation via inference in a cnn-based higher-order spatio-temporal mrf. In *Proceedings of the IEEE conference on computer vision and pattern recognition*, pages 5977–5986, 2018. 6
- [2] Zhipeng Bao, Pavel Tokmakov, Allan Jabri, Yu-Xiong Wang, Adrien Gaidon, and Martial Hebert. Discovering objects that can move. In *Proceedings of the IEEE/CVF Conference on Computer Vision and Pattern Recognition (CVPR)*, pages 11789–11798, June 2022. 8
- [3] Daniel Bear, Chaofei Fan, Damian Mrowca, Yunzhu Li, Seth Alter, Aran Nayebi, Jeremy Schwartz, Li F Fei-Fei, Jiajun Wu, Josh Tenenbaum, et al. Learning physical graph representations from visual scenes. *Advances in Neural Information Processing Systems*, 33:6027–6039, 2020. 8
- [4] Beril Besbinar and Pascal Frossard. Self-supervision by prediction for object discovery in videos. In *2021 IEEE International Conference on Image Processing (ICIP)*, pages 1509–1513. IEEE, 2021. 8
- [5] Thomas Brox and Jitendra Malik. Object segmentation by long term analysis of point trajectories. In *European conference on computer vision*, pages 282–295. Springer, 2010. 8
- [6] Christopher P Burgess, Loic Matthey, Nicholas Watters, Rishabh Kabra, Irina Higgins, Matt Botvinick, and Alexander Lerchner. Monet: Unsupervised scene decomposition and representation. *arXiv preprint arXiv:1901.11390*, 2019. 8
- [7] Sergi Caelles, Kevis-Kokitsi Maninis, Jordi Pont-Tuset, Laura Leal-Taixé, Daniel Cremers, and Luc Van Gool. One-shot video object segmentation. In *Proceedings of the IEEE conference on computer vision and pattern recognition*, pages 221–230, 2017. 6
- [8] Hu Cao, Yueyue Wang, Joy Chen, Dongsheng Jiang, Xiaopeng Zhang, Qi Tian, and Manning Wang. Swin-UNET: UNet-like pure transformer for medical image segmentation. *arXiv preprint arXiv:2105.05537*, 2021. 5
- [9] Mathilde Caron, Hugo Touvron, Ishan Misra, Hervé Jégou, Julien Mairal, Piotr Bojanowski, and Armand Joulin. Emerging properties in self-supervised vision transformers. In *Proceedings of the IEEE/CVF International Conference on Computer Vision*, pages 9650–9660, 2021. 5
- [10] Kyunghyun Cho, Bart van Merriënboer, Çaglar Gülçehre, Dzmitry Bahdanau, Fethi Bougares, Holger Schwenk, and Yoshua Bengio. Learning phrase representations using rnn encoder-decoder for statistical machine translation. In *EMNLP*, 2014. 4
- [11] Subhabrata Choudhury, Laurynas Karazija, Iro Laina, Andrea Vedaldi, and Christian Ruppert. Guess what moves:

- Unsupervised video and image segmentation by anticipating motion. *arXiv preprint arXiv:2205.07844*, 2022. 8
- [12] Eric Crawford and Joelle Pineau. Spatially invariant unsupervised object detection with convolutional neural networks. In *Proceedings of the AAAI Conference on Artificial Intelligence*, volume 33, pages 3412–3420, 2019. 8
- [13] Eric Crawford and Joelle Pineau. Exploiting spatial invariance for scalable unsupervised object tracking. In *Proceedings of the AAAI Conference on Artificial Intelligence*, volume 34, pages 3684–3692, 2020. 8
- [14] Suyog Dutt Jain, Bo Xiong, and Kristen Grauman. Fusion-seg: Learning to combine motion and appearance for fully automatic segmentation of generic objects in videos. In *Proceedings of the IEEE conference on computer vision and pattern recognition*, pages 3664–3673, 2017. 6, 7
- [15] Patrick Emami, Pan He, Sanjay Ranka, and Anand Rangarajan. Efficient iterative amortized inference for learning symmetric and disentangled multi-object representations. In *International Conference on Machine Learning*, pages 2970–2981. PMLR, 2021. 8
- [16] Martin Engelcke, Adam R Kosiorek, Oiwi Parker Jones, and Ingmar Posner. Genesis: Generative scene inference and sampling with object-centric latent representations. *arXiv preprint arXiv:1907.13052*, 2019. 8
- [17] Martin Engelcke, Oiwi Parker Jones, and Ingmar Posner. Genesis-v2: Inferring unordered object representations without iterative refinement. *Advances in Neural Information Processing Systems*, 34:8085–8094, 2021. 8
- [18] Alon Faktor and Michal Irani. Video segmentation by non-local consensus voting. In *BMVC*, volume 2, page 8, 2014. 7
- [19] Deng-Ping Fan, Wenguan Wang, Ming-Ming Cheng, and Jianbing Shen. Shifting more attention to video salient object detection. In *Proceedings of the IEEE/CVF conference on computer vision and pattern recognition*, pages 8554–8564, 2019. 6
- [20] Katerina Fragkiadaki, Geng Zhang, and Jianbo Shi. Video segmentation by tracing discontinuities in a trajectory embedding. In *2012 IEEE Conference on Computer Vision and Pattern Recognition*, pages 1846–1853. IEEE, 2012. 8
- [21] James Jerome Gibson and Leonard Carmichael. *The senses considered as perceptual systems*, volume 2. Houghton Mifflin Boston, 1966. 1
- [22] Klaus Greff, Raphaël Lopez Kaufman, Rishabh Kabra, Nick Watters, Christopher Burgess, Daniel Zoran, Loic Matthey, Matthew Botvinick, and Alexander Lerchner. Multi-object representation learning with iterative variational inference. In *International Conference on Machine Learning*, pages 2424–2433. PMLR, 2019. 8
- [23] Yuan-Ting Hu, Jia-Bin Huang, and Alexander Schwing. Maskrnn: Instance level video object segmentation. *Advances in neural information processing systems*, 30, 2017. 6
- [24] Yuan-Ting Hu, Jia-Bin Huang, and Alexander G Schwing. Videomatch: Matching based video object segmentation. In *Proceedings of the European conference on computer vision (ECCV)*, pages 54–70, 2018. 6
- [25] Allan Jabri, Andrew Owens, and Alexei Efros. Space-time correspondence as a contrastive random walk. *Advances in neural information processing systems*, 33:19545–19560, 2020. 5, 6, 12
- [26] Jindong Jiang and Sungjin Ahn. Generative neurosymbolic machines. *Advances in Neural Information Processing Systems*, 33:12572–12582, 2020. 8
- [27] Jindong Jiang, Sepehr Janghorbani, Gerard De Melo, and Sungjin Ahn. Scalor: Generative world models with scalable object representations. *arXiv preprint arXiv:1910.02384*, 2019. 8
- [28] Joakim Johnander, Martin Danelljan, Emil Brissman, Fahad Shahbaz Khan, and Michael Felsberg. A generative appearance model for end-to-end video object segmentation. In *Proceedings of the IEEE/CVF Conference on Computer Vision and Pattern Recognition*, pages 8953–8962, 2019. 6
- [29] Rishabh Kabra, Daniel Zoran, Goker Erdogan, Loic Matthey, Antonia Creswell, Matt Botvinick, Alexander Lerchner, and Chris Burgess. Simone: View-invariant, temporally-abstracted object representations via unsupervised video decomposition. *Advances in Neural Information Processing Systems*, 34:20146–20159, 2021. 8
- [30] Margret Keuper, Bjoern Andres, and Thomas Brox. Motion trajectory segmentation via minimum cost multicuts. In *Proceedings of the IEEE international conference on computer vision*, pages 3271–3279, 2015. 8
- [31] Thomas Kipf, Gamaleldin Fathy Elsayed, Aravindh Mahendran, Austin Stone, Sara Sabour, Georg Heigold, Rico Jonckhowski, Alexey Dosovitskiy, and Klaus Greff. Conditional object-centric learning from video. In *International Conference on Learning Representations*, 2022. 6, 8
- [32] Adam Kosiorek, Hyunjik Kim, Yee Whye Teh, and Ingmar Posner. Sequential attend, infer, repeat: Generative modelling of moving objects. *Advances in Neural Information Processing Systems*, 31, 2018. 8
- [33] John Lafferty, Andrew McCallum, and Fernando CN Pereira. Conditional random fields: Probabilistic models for segmenting and labeling sequence data. 2001. 5
- [34] Zihang Lai, Erika Lu, and Weidi Xie. Mast: A memory-augmented self-supervised tracker. In *Proceedings of the IEEE/CVF Conference on Computer Vision and Pattern Recognition*, pages 6479–6488, 2020. 6, 12
- [35] Z. Lai and W. Xie. Self-supervised learning for video correspondence flow. In *BMVC*, 2019. 6
- [36] Hala Lamdouar, Weidi Xie, and Andrew Zisserman. Segmenting invisible moving objects. In *British Machine Vision Association*, 2021. 5, 7
- [37] José Lezama, Karteek Alahari, Josef Sivic, and Ivan Laptev. Track to the future: Spatio-temporal video segmentation with long-range motion cues. In *CVPR 2011*, pages 3369–3376. IEEE, 2011. 8
- [38] Fuxin Li, Taeyoung Kim, Ahmad Humayun, David Tsai, and James M Rehg. Video segmentation by tracking many figure-ground segments. In *Proceedings of the IEEE international conference on computer vision*, pages 2192–2199, 2013. 2, 5
- [39] Xueting Li, Sifei Liu, Shalini De Mello, Xiaolong Wang, Jan Kautz, and Ming-Hsuan Yang. Joint-task self-supervised

- learning for temporal correspondence. In H. Wallach, H. Larochelle, A. Beygelzimer, F. d'Alché-Buc, E. Fox, and R. Garnett, editors, *Advances in Neural Information Processing Systems*, volume 32. Curran Associates, Inc., 2019. 6
- [40] Xiaoxiao Li and Chen Change Loy. Video object segmentation with joint re-identification and attention-aware mask propagation. In *Proceedings of the European conference on computer vision (ECCV)*, pages 90–105, 2018. 6
- [41] Zhixuan Lin, Yi-Fu Wu, Skand Vishwanath Peri, Weihao Sun, Gautam Singh, Fei Deng, Jindong Jiang, and Sungjin Ahn. Space: Unsupervised object-oriented scene representation via spatial attention and decomposition. *arXiv preprint arXiv:2001.02407*, 2020. 8
- [42] Runtao Liu, Zhirong Wu, Stella Yu, and Stephen Lin. The emergence of objectness: Learning zero-shot segmentation from videos. In M. Ranzato, A. Beygelzimer, Y. Dauphin, P.S. Liang, and J. Wortman Vaughan, editors, *Advances in Neural Information Processing Systems*, volume 34, pages 13137–13152. Curran Associates, Inc., 2021. 1, 7, 8
- [43] Francesco Locatello, Dirk Weissenborn, Thomas Unterthiner, Aravindh Mahendran, Georg Heigold, Jakob Uszkoreit, Alexey Dosovitskiy, and Thomas Kipf. Object-centric learning with slot attention. *Advances in Neural Information Processing Systems*, 33:11525–11538, 2020. 3, 8
- [44] Ilya Loshchilov and Frank Hutter. Decoupled weight decay regularization. In *International Conference on Learning Representations*, 2018. 5
- [45] Xiankai Lu, Wenguan Wang, Chao Ma, Jianbing Shen, Ling Shao, and Fatih Porikli. See more, know more: Unsupervised video object segmentation with co-attention siamese networks. In *Proceedings of the IEEE/CVF conference on computer vision and pattern recognition*, pages 3623–3632, 2019. 7
- [46] Xiankai Lu, Wenguan Wang, Jianbing Shen, Yu-Wing Tai, David J. Crandall, and Steven C. H. Hoi. Learning video object segmentation from unlabeled videos. In *Proceedings of the IEEE/CVF Conference on Computer Vision and Pattern Recognition (CVPR)*, June 2020. 6
- [47] K-K Maninis, Sergi Caelles, Yuhua Chen, Jordi Pont-Tuset, Laura Leal-Taixé, Daniel Cremers, and Luc Van Gool. Video object segmentation without temporal information. *IEEE transactions on pattern analysis and machine intelligence*, 41(6):1515–1530, 2018. 6
- [48] N. Mayer, E. Ilg, P. Häusser, P. Fischer, D. Cremers, A. Dosovitskiy, and T. Brox. A large dataset to train convolutional networks for disparity, optical flow, and scene flow estimation. In *IEEE International Conference on Computer Vision and Pattern Recognition (CVPR)*, 2016. arXiv:1512.02134. 5
- [49] Cheol-Hui Min, Jinseok Bae, Junho Lee, and Young Min Kim. Gatsbi: Generative agent-centric spatio-temporal object interaction. In *Proceedings of the IEEE/CVF Conference on Computer Vision and Pattern Recognition*, pages 3074–3083, 2021. 8
- [50] Peter Ochs and Thomas Brox. Higher order motion models and spectral clustering. In *2012 IEEE Conference on Computer Vision and Pattern Recognition*, pages 614–621. IEEE, 2012. 8
- [51] Peter Ochs, Jitendra Malik, and Thomas Brox. Segmentation of moving objects by long term video analysis. *IEEE transactions on pattern analysis and machine intelligence*, 36(6):1187–1200, 2013. 2, 5, 8
- [52] Seoung Wug Oh, Joon-Young Lee, Ning Xu, and Seon Joo Kim. Video object segmentation using space-time memory networks. In *Proceedings of the IEEE/CVF International Conference on Computer Vision*, pages 9226–9235, 2019. 6
- [53] Federico Perazzi, Anna Khoreva, Rodrigo Benenson, Bernt Schiele, and Alexander Sorkine-Hornung. Learning video object segmentation from static images. In *Proceedings of the IEEE conference on computer vision and pattern recognition*, pages 2663–2672, 2017. 6
- [54] Federico Perazzi, Jordi Pont-Tuset, Brian McWilliams, Luc Van Gool, Markus Gross, and Alexander Sorkine-Hornung. A benchmark dataset and evaluation methodology for video object segmentation. In *Proceedings of the IEEE conference on computer vision and pattern recognition*, pages 724–732, 2016. 2, 5
- [55] Christian Schmidt, Ali Athar, Sabarinath Mahadevan, and Bastian Leibe. D2conv3d: Dynamic dilated convolutions for object segmentation in videos. In *Proceedings of the IEEE/CVF Winter Conference on Applications of Computer Vision*, pages 1200–1209, 2022. 7
- [56] Deqing Sun, Xiaodong Yang, Ming-Yu Liu, and Jan Kautz. Pwc-net: Cnns for optical flow using pyramid, warping, and cost volume. In *Proceedings of the IEEE conference on computer vision and pattern recognition*, pages 8934–8943, 2018. 4
- [57] Zachary Teed and Jia Deng. Raft: Recurrent all-pairs field transforms for optical flow. In *European conference on computer vision*, pages 402–419. Springer, 2020. 1, 4, 5
- [58] Joshua B Tenenbaum, Charles Kemp, Thomas L Griffiths, and Noah D Goodman. How to grow a mind: Statistics, structure, and abstraction. *science*, 331(6022):1279–1285, 2011. 1
- [59] Pavel Tokmakov, Karteek Alahari, and Cordelia Schmid. Learning motion patterns in videos. In *Proceedings of the IEEE conference on computer vision and pattern recognition*, pages 3386–3394, 2017. 8
- [60] Pavel Tokmakov, Karteek Alahari, and Cordelia Schmid. Learning video object segmentation with visual memory. In *Proceedings of the IEEE International Conference on Computer Vision*, pages 4481–4490, 2017. 8
- [61] Ashish Vaswani, Noam Shazeer, Niki Parmar, Jakob Uszkoreit, Llion Jones, Aidan N Gomez, Łukasz Kaiser, and Illia Polosukhin. Attention is all you need. *Advances in neural information processing systems*, 30, 2017. 5
- [62] Paul Voigtlaender, Yuning Chai, Florian Schroff, Hartwig Adam, Bastian Leibe, and Liang-Chieh Chen. Feelvos: Fast end-to-end embedding learning for video object segmentation. In *Proceedings of the IEEE/CVF Conference on Computer Vision and Pattern Recognition*, pages 9481–9490, 2019. 6

- [63] Carl Vondrick, Abhinav Shrivastava, Alireza Fathi, Sergio Guadarrama, and Kevin Murphy. Tracking emerges by colorizing videos. In *Proceedings of the European conference on computer vision (ECCV)*, pages 391–408, 2018. 6
- [64] Ning Wang, Yibing Song, Chao Ma, Wengang Zhou, Wei Liu, and Houqiang Li. Unsupervised deep tracking. In *Proceedings of the IEEE/CVF Conference on Computer Vision and Pattern Recognition*, pages 1308–1317, 2019. 6
- [65] Wenguan Wang, Jianbing Shen, Ruigang Yang, and Fatih Porikli. Saliency-aware video object segmentation. *IEEE transactions on pattern analysis and machine intelligence*, 40(1):20–33, 2017. 7
- [66] Max Wertheimer. Untersuchungen zur lehre von der gestalt. ii. *Psychologische forschung*, 4(1):301–350, 1923. 1
- [67] Christopher Xie, Yu Xiang, Zaid Harchaoui, and Dieter Fox. Object discovery in videos as foreground motion clustering. In *Proceedings of the IEEE/CVF Conference on Computer Vision and Pattern Recognition*, pages 9994–10003, 2019. 8
- [68] Junyu Xie, Weidi Xie, and Andrew Zisserman. Segmenting moving objects via an object-centric layered representation. *arXiv preprint arXiv:2207.02206*, 2022. 5, 6, 7, 8, 12
- [69] Jiarui Xu and Xiaolong Wang. Rethinking self-supervised correspondence learning: A video frame-level similarity perspective. In *Proceedings of the IEEE/CVF International Conference on Computer Vision*, pages 10075–10085, 2021. 6
- [70] Charig Yang, Hala Lamdouar, Erika Lu, Andrew Zisserman, and Weidi Xie. Self-supervised video object segmentation by motion grouping. In *Proceedings of the IEEE/CVF International Conference on Computer Vision (ICCV)*, pages 7177–7188, October 2021. 1, 2, 3, 5, 6, 7, 8, 14, 15
- [71] Yanchao Yang, Brian Lai, and Stefano Soatto. Dystab: Unsupervised object segmentation via dynamic-static bootstrapping. In *Proceedings of the IEEE/CVF Conference on Computer Vision and Pattern Recognition (CVPR)*, pages 2826–2836, June 2021. 1
- [72] Yanchao Yang, Antonio Loquercio, Davide Scaramuzza, and Stefano Soatto. Unsupervised moving object detection via contextual information separation. In *Proceedings of the IEEE/CVF Conference on Computer Vision and Pattern Recognition (CVPR)*, June 2019. 1, 3, 5, 7, 8
- [73] Vickie Ye, Zhengqi Li, Richard Tucker, Angjoo Kanazawa, and Noah Snavely. Deformable sprites for unsupervised video decomposition. In *IEEE Conference on Computer Vision and Pattern Recognition (CVPR)*, June 2022. 8
- [74] Polina Zablotkaia, Edoardo A Dominici, Leonid Sigal, and Andreas M Lehrmann. Unsupervised video decomposition using spatio-temporal iterative inference. *arXiv preprint arXiv:2006.14727*, 2020. 8
- [75] Tianfei Zhou, Shunzhou Wang, Yi Zhou, Yazhou Yao, Jianwu Li, and Ling Shao. Motion-attentive transition for zero-shot video object segmentation. In *Proceedings of the AAAI Conference on Artificial Intelligence*, volume 34, pages 13066–13073, 2020. 7
- [76] Xizhou Zhu, Han Hu, Stephen Lin, and Jifeng Dai. Deformable convnets v2: More deformable, better results. In *Proceedings of the IEEE/CVF conference on computer vision and pattern recognition*, pages 9308–9316, 2019. 3

A. More Implementation Details

In this section, we list the architecture details and training settings. Codes and models will be released publicly.

A.1. Visual Encoder

The visual encoder contains the first three stages of Swin-Tiny V2. We tabulate the workflow in Table 3.

stage	operation	output sizes
input	-	$3 \times 192 \times 384$
PatchEmbed	4×4 , stride 4, 96	$96 \times 48 \times 96$
SwinBlock1	$\begin{bmatrix} h = 3 \\ ws = 12 \end{bmatrix} \times 2$	$96 \times 48 \times 96$
DownSample1	192	$192 \times 24 \times 48$
SwinBlock2	$\begin{bmatrix} h = 6 \\ ws = 12 \end{bmatrix} \times 2$	$192 \times 24 \times 48$
DownSample2	384	$384 \times 12 \times 24$
SwinBlock3	$\begin{bmatrix} h = 12 \\ ws = 12 \end{bmatrix} \times 6$	$384 \times 12 \times 24$

Table 3. Architecture of visual encoder. h stands for the number of attention heads while ws refers to window size.

A.2. Frame Comparator

The frame comparator possesses two deformable convolutional layers, with ReLU operation in between and three Transformer Encoder blocks. We tabulate the workflow in Table 4.

stage	operation	output sizes
input	-	$768 \times 12 \times 24$
DeformConv1	3×3 , 768	$768 \times 12 \times 24$
ReLU	-	$768 \times 12 \times 24$
DeformConv2	3×3 , 384	$384 \times 12 \times 24$
Transformer	$\begin{bmatrix} h = 8 \\ 384 \end{bmatrix} \times 3$	$384 \times 12 \times 24$

Table 4. Architecture of frame comparator. h represents the number of attention heads

A.3. Flow Decoder

The frame comparator consists of three stages of SwinV2 block added with linear expanding layers. We tabulate the workflow in Table 5.

A.4. Training Details

For all datasets, we train with a batch size of 2. To train more efficiently, we sample three flow pairs ($i \rightarrow j$) for a given frame i ; one is static replication $i = j$, another two are motion pair $i \neq j$. We apply temporal consistency first

stage	operation	output sizes
input	-	$384 \times 12 \times 24$
SwinBlock1	$\begin{bmatrix} h = 12 \\ ws = 12 \end{bmatrix} \times 2$	$384 \times 12 \times 24$
PatchExpand1	768	$192 \times 24 \times 48$
SwinBlock2	$\begin{bmatrix} h = 6 \\ ws = 12 \end{bmatrix} \times 2$	$192 \times 24 \times 48$
PatchExpand2	384	$96 \times 48 \times 96$
SwinBlock3	$\begin{bmatrix} h = 3 \\ ws = 12 \end{bmatrix} \times 2$	$96 \times 48 \times 96$
PatchExpand3	1536	$96 \times 192 \times 384$
outConv	5×5 , stride 1, 4	$4 \times 192 \times 384$

Table 5. Architecture of flow decoder. h stands for the number of attention heads while ws refers to window size.

on the masks from two motion pairs, then pull the static mask to the average of two dynamic masks closer. We linearly warm up the learning rate for the first 1k iterations. Besides, for every 100k iterations, we decay the learning rate by half and increase the scale of temporal consistency λ_c and entropy regularisation λ_e by the factor of 5. In the default setting, we train for about 3 days on 8 standard Tesla V100 GPUs with 32GB memory each.

A.5. Test-time Adaptation

Inspired by OCLR [68], we adopt test-time adaptation based on RGB sequence to enhance appearance consistency. In detail, we follow existing works on self-supervised tracking [25, 34] to propagate object masks across time span. The whole process consists of three steps. First, we extract RGB features of each frame with a DINO-pretrained ViT encoder. Then, we select key frames for object mask propagation. Finally, we calculate the affinity matrix between frames and perform mask propagation.

DINO Feature Extraction. Given a video sequence $v = \{x_1, \dots, x_T\}$, $v \in \mathbb{R}^{T \times H \times W \times 3}$, we use DINO pretrained ViT-Small encoder with patch size 8×8 to extract features:

$$\{f_1, \dots, f_T\} = \{\Phi(x_1), \dots, \Phi(x_T)\}, \quad (14)$$

where $f_t \in \mathbb{R}^{h \times w \times 384}$, $h = H//8$ and $w = W//8$. The extracted features will be used in the mask propagation step.

Key Frame Selection. Given video v , our model predicts object mask of each frame as $m = \{\alpha_1, \dots, \alpha_T\}$, $m \in \mathbb{R}^{T \times H \times W \times 1}$. Since the video frames are continuous along the temporal dimension, it is practical to propagate object masks between neighboring frames. The propagation operation is the same as [25], the only difference is that we have no ground-truth mask for reference. Therefore, we need to design a mechanism to select object masks of high confidence. To do this, we measure the temporal coherence of

predicted object masks for key frame selection. Specifically, for each timestamp $t \in \{3, \dots, T-2\}$, we can calculate four propagated masks as:

$$\hat{\alpha}_t = [\text{Mask-prop}(\alpha_{t-i})]_{i \in \{-2, -1, 1, 2\}}, \quad (15)$$

where ‘Mask-prop’ denotes the propagation operation. Then we calculate the average IoU between the original mask and propagated masks as the confidence score:

$$s_t = \frac{1}{4} \sum_{i=0}^3 \text{IoU}(\hat{\alpha}_t[i], \alpha_t). \quad (16)$$

The calculated s_t measures the coherency between α_t and its neighbors. Our empirical studies show that it serves as a reliable signal for key frame selection.

Object Mask Propagation. We select timestamps with Top- $k\%$ confidence score as the key reference frames ($k = 15$ on DAVIS2016, $k = 25$ on SegTrackv2, $k = 10$ on FBMS-59). Then we iteratively propagate the object masks with a neighbor temporal window size $n = 7$.

B. Results Breakdown

We include a specific result breakdown in this section. We show the per-sequence results on DAVIS2016 in Table 6, SegTrackv2 in Table 7 and FBMS-59 in Table 8.

Sequence	\mathcal{J} (Mean) \uparrow	
	w/o post proc.	test-time adap.
dog	80.7	87.4
cows	87.2	88.8
goat	47.5	80.6
camel	85.6	86.1
libby	72.5	77.7
parkour	72.9	87.9
soapbox	84.6	86.5
blackswan	48.9	46.9
bmx-trees	50.1	55.8
kite-surf	55.9	62.6
car-shadow	87.9	86.9
breakdance	82.6	76.0
dance-twirl	82.5	85.4
scooter-black	80.2	80.3
drift-chicane	78.6	82.2
motocross-jump	68.4	88.9
horsejump-high	78.0	84.3
drift-straight	69.2	80.0
car-roundabout	87.7	83.9
paragliding-launch	62.1	62.8
frame avg.	73.9	79.2

Table 6. Sequence-wise results on DAVIS2016.

Sequence	\mathcal{J} (Mean) \uparrow	
	w/o post proc.	test-time adap.
drift	41.7	40.7
birdfall	38.2	61.5
girl	76.5	82.3
cheetah	18.4	30.1
worm	52.5	74.3
parachute	90.2	92.0
monkeydog	14.3	31.1
hummingbird	61.2	58.8
soldier	66.3	58.8
bmw	73.7	78.8
frog	80.5	76.3
penguin	63.5	62.7
monkey	46.8	77.4
bird of paradise	85.3	85.4
frame avg.	62.2	69.4

Table 7. Sequence-wise results on SegTrackv2.

C. More Qualitative Results

We show more qualitative results of SegTrackv2 and FBMS-59 in Figure 4 and Figure 5.

Sequence	\mathcal{J} (Mean) \uparrow	
	w/o post proc.	test-time adap.
camel01	25.8	66.9
cars1	66.1	88.3
cars10	31.6	33.9
cars4	72.9	83.2
cars5	81.2	82.5
cats01	80.6	79.2
cats03	62.0	63.4
cats06	40.1	38.7
dogs01	70.6	61.2
dogs02	62.8	82.2
farm01	86.7	88.9
giraffes01	38.6	52.2
goats01	44.8	45.3
horses02	64.4	77.6
horses04	68.5	73.5
horses05	43.7	49.0
lion01	60.1	71.5
marple12	74.7	80.3
marple2	65.0	71.4
marple4	79.1	91.6
marple6	76.0	85.1
marple7	72.5	55.2
marple9	87.5	97.9
people03	76.5	48.5
people1	72.4	80.8
people2	80.9	83.0
rabbits02	50.2	58.9
rabbits03	39.5	55.7
rabbits04	47.0	53.0
tennis	63.1	71.1
frame avg.	61.3	66.9

Table 8. Sequence-wise results on FBMS-59.

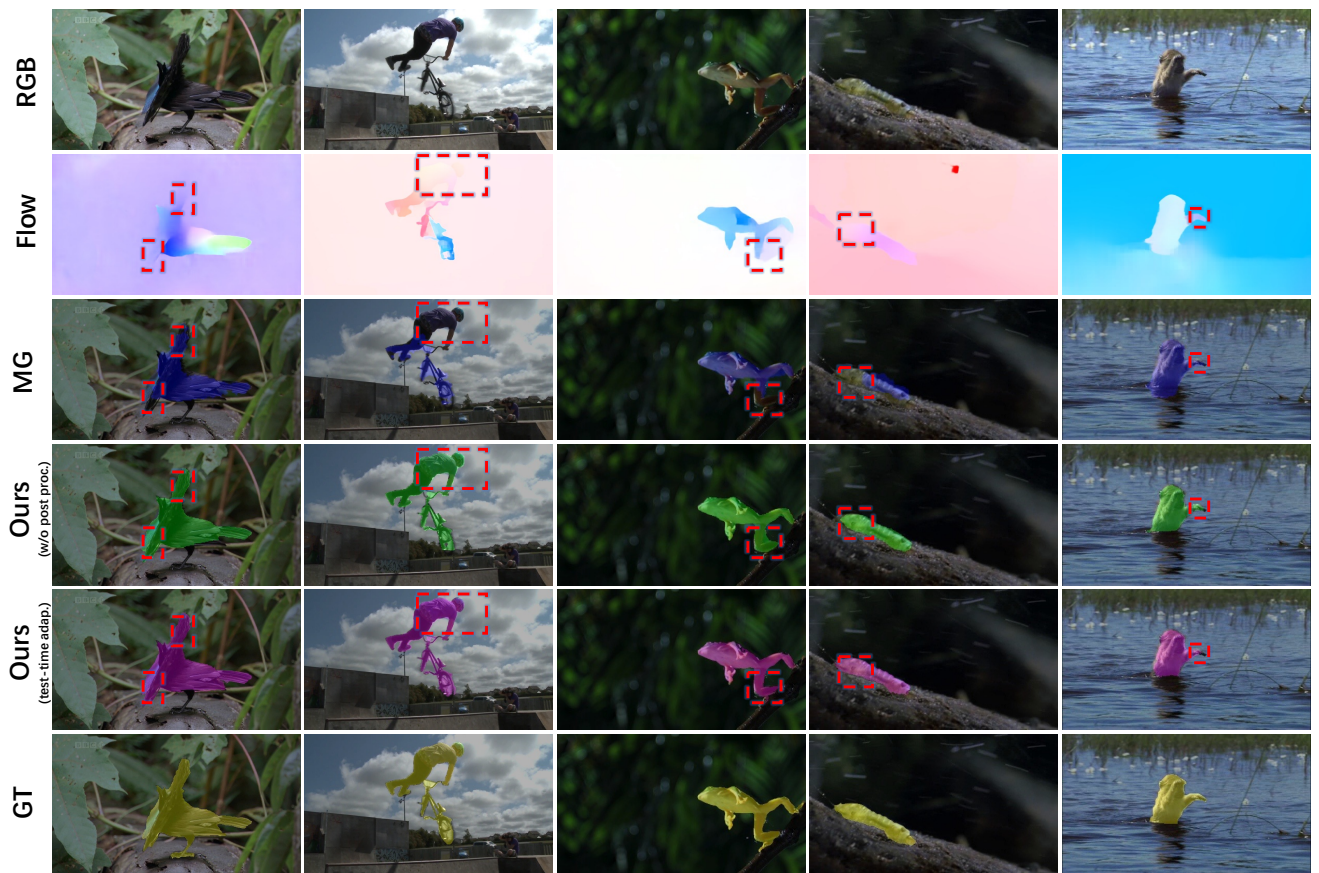


Figure 4. Qualitative results on SegTrackv2. MG refers to [70]. Red boxes outline the corresponding difference.

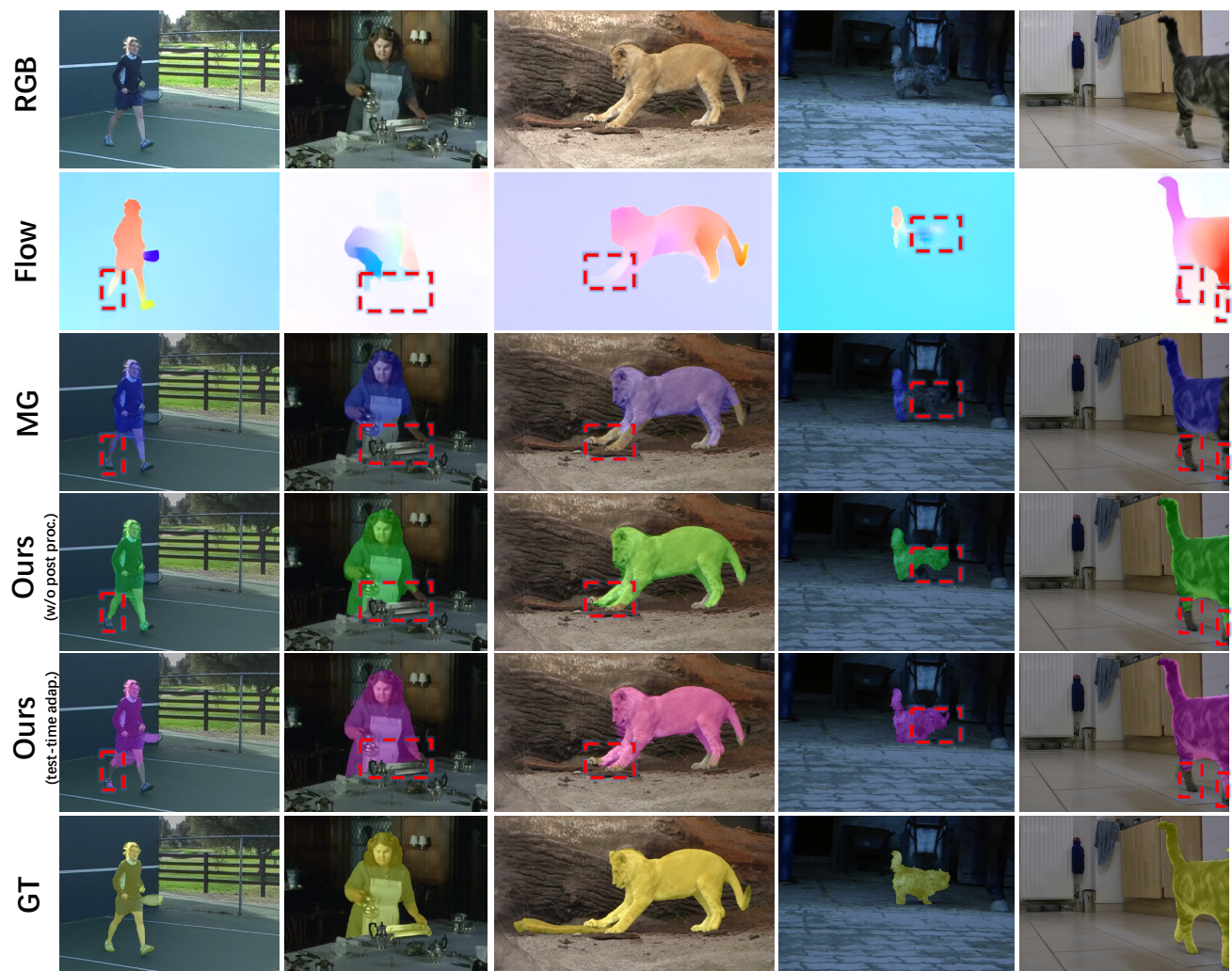


Figure 5. Qualitative results on FBMS-59. MG refers to [70]. Red boxes highlight the corresponding difference.